

Source Localization and Sensing: A Nonparametric Iterative Adaptive Approach Based on Weighted Least Squares

TARIK YARDIBI, Student Member, IEEE

JIAN LI, Fellow, IEEE
University of Florida

PETRE STOICA, Fellow, IEEE
Uppsala University
Sweden

MING XUE, Student Member, IEEE
University of Florida

ARTHUR B. BAGGEROER, Fellow, IEEE
Massachusetts Institute of Technology

Array processing is widely used in sensing applications for estimating the locations and waveforms of the sources in a given field. In the absence of a large number of snapshots, which is the case in numerous practical applications, such as underwater array processing, it becomes challenging to estimate the source parameters accurately. This paper presents a nonparametric and hyperparameter, free-weighted, least squares-based iterative adaptive approach for amplitude and phase estimation (IAA-APES) in array processing. IAA-APES can work well with few snapshots (even one), uncorrelated, partially correlated, and coherent sources, and arbitrary array geometries. IAA-APES is extended to give sparse results via a model-order selection tool, the Bayesian information criterion (BIC). Moreover, it is shown that further improvements in resolution and accuracy can be achieved by applying the parametric relaxation-based cyclic approach (RELAX) to refine the IAA-APES&BIC estimates if desired. IAA-APES can also be applied to active sensing applications, including single-input single-output (SISO) radar/sonar range-Doppler imaging and multi-input single-output (MISO) channel estimation for communications. Simulation results are presented to evaluate the performance of IAA-APES for all of these applications, and IAA-APES is shown to outperform a number of existing approaches.

Manuscript received December 11, 2007; revised July 21 and November 4, 2008; released for publication November 16, 2008.

IEEE Log No. T-AES/46/1/935952.

Refereeing of this contribution was handled by W. Koch.

This work was supported in part by the Office of Naval Research (ONR) under Grants N00014-07-1-0193, N00014-07-1-0293, and N00014-01-1-0257, the Army Research Office (ARO) under Grant W911NF-07-1-0450, the National Aeronautics and Space Administration (NASA) under Grant NNX07AO15A, the National Science Foundation (NSF) under Grants CCF-0634786, ECS-0621879, and ECS-0729727, the Swedish Research Council (VR), and the European Research Council (ERC).

Opinions, interpretations, conclusions, and recommendations are those of the authors and are not necessarily endorsed by the United States Government.

Authors' addresses: T. Yardibi, J. Li, M. Xue, Dept. of Electrical and Computer Engineering, University of Florida, PO Box 116130, Gainesville, FL 32611, E-mail: (li@dsp.ufl.edu); P. Stoica, Dept. of Information Technology, Uppsala University, Uppsala, Sweden; A. B. Baggeroer, Depts. of Mechanical Engineering & Electrical Engineering and Computer Science, Massachusetts Institute of Technology, Cambridge, MA 02139.

0018-9251/10/\$26.00 © 2010 IEEE

I. INTRODUCTION

The goal of array processing is to estimate the locations and waveforms of sources by combining the received data from multiple sensors so that the desired signal is enhanced, while the unwanted signals, such as interference and noise, are suppressed. In active sensing applications such as radar/sonar range-Doppler imaging, the aim is to find targets present in a region of interest. For channel estimation in communications, the aim is to estimate the non-zero channel taps and their Doppler shifts, which are then fed to the subsequent equalizer for symbol detection. Low numbers of snapshots and low signal-to-noise ratios (SNR) are among the many challenges that array processing systems frequently face. Another challenge is the presence of nearby sources, in terms of location or Doppler, since closely spaced sources are harder to discriminate. Herein both passive array processing and active sensing are considered.

The most basic approach to array processing is the classical delay-and-sum (DAS) method, in which the received signal from each sensor is weighted and delayed so as to focus on different points in space. However, this method suffers from low resolution and high sidelobe levels. There is a vast amount of literature on methods that provide superior performance over the DAS approach when certain assumptions are met [1]. The well-known standard Capon beamformer (SCB) [2] and multiple signal classification (MUSIC) [3, 4] methods provide superresolution when the sources are uncorrelated and the number of snapshots is high. Many extensions to these methods have been proposed to deal with modelling errors, such as steering vector mismatches. (See, e.g., [5]–[9].) However, none of these methods is able to cope with very low snapshot numbers, coherent or highly correlated sources, or severe noise.

Only a few snapshots are available when the environment being sensed by the array is stationary for a short duration of time. Moreover, to avoid smearing, i.e., losing resolution because of wide main beamwidths in the array response, averaging can only be done over a small bandwidth [10, 11]. Therefore the number of available snapshots, which is directly related to the time-bandwidth product, can be very small, sometimes as small as 3, for applications such as underwater array processing. Furthermore, as discussed later, the data models for single-input single-output (SISO) radar/sonar range-Doppler imaging and multi-input single-output (MISO) channel estimation in communication problems are similar to the model used in array processing with a single snapshot and an arbitrary array geometry (dictated by the probing waveforms).

The array processing problem has been carried into the sparse signal representation area by noticing that the number of actual sources is usually much smaller

TABLE I
Notation used in the Text

$\ \cdot\ _0$	ℓ_0 -norm
$\ \cdot\ _1$	ℓ_1 -norm
$\ \cdot\ _2$	ℓ_2 -norm
$\ \cdot\ _F$	Frobenius norm of a matrix
\odot	the Hadamard (elementwise) matrix product
$\text{tr}(\cdot)$	trace of a matrix
$(\cdot)^T$	transpose of a vector or matrix
$(\cdot)^H$	conjugate transpose of a vector or matrix

than the number of potential source points that can be considered [12–29]. Sparsity-based techniques have also been used in spectral estimation [30], image processing, and array design [31–33], among many other application areas. Sparse signal representation algorithms can deal with a few snapshots (even one). However, they may require large computation times and the fine tuning of one or more hyperparameters.

Application areas, ranging from passive source localization to active radar/sonar range-Doppler imaging and channel estimation for communications are addressed here. Section II considers passive sensing applications and describes a weighted least squares-based iterative adaptive approach for amplitude and phase estimation (IAA-APES). The algorithm is named IAA-APES herein since its derivation resembles that of the amplitude and phase estimation (APES) algorithm [34–36]. (See Section IIC.) This name also distinguishes it from the maximum likelihood (ML)-based iterative adaptive approach (IAA-ML) discussed in the Appendix to further motivate IAA-APES. Using the Bayesian information criterion (BIC) [37, 38], IAA-APES can be extended to yield point source estimates. (This approach is referred to as IAA-APES&BIC.) Next, a parametric relaxation-based cyclic approach, namely RELAX [39, 40], is discussed as a way to further refine the results of IAA-APES&BIC. (This approach is referred to as IAA-APES&RELAX.) Section III presents the data models for the aforementioned active sensing applications and emphasizes the similarities to the passive sensing case. IAA-APES is evaluated via comprehensive simulations in Section IV, and the IAA-APES’ performance is compared with that of a number of existing approaches.

Notation: We denote vectors and matrices by boldface lowercase and boldface uppercase letters, respectively. The k th component of a vector \mathbf{x} is written as x_k . The k th diagonal element of a matrix \mathbf{P} is written as P_k . See Table I for other symbols and their meanings.

II. PASSIVE SENSING

In passive sensing applications such as aeroacoustic noise measurements [41] and underwater acoustic measurements [42], an array of sensors is

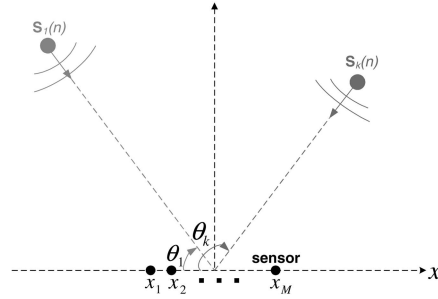


Fig. 1. Far-field linear array.

used to estimate the desired source characteristics. This section first introduces the data model for such applications and then the IAA-APES algorithm in this model.

A. Data Model

Consider the wavefield generated by K sources located at $\boldsymbol{\theta}$, where $\boldsymbol{\theta} \triangleq [\theta_1, \theta_2, \dots, \theta_K]$ and θ_k are the location parameters of the k th signal, $k = 1, \dots, K$. In the narrowband, multi-snapshot case, the $M \times 1$ array output vector of an M element array in the presence of additive noise can be represented as [5, 43]

$$\mathbf{y}(n) = \mathbf{A}(\boldsymbol{\theta})\mathbf{s}(n) + \mathbf{e}(n), \quad n = 1, \dots, N \quad (1)$$

where N is the number of snapshots, $\mathbf{A}(\boldsymbol{\theta})$ is the $M \times K$ steering matrix defined as $\mathbf{A}(\boldsymbol{\theta}) \triangleq [\mathbf{a}(\theta_1), \mathbf{a}(\theta_2), \dots, \mathbf{a}(\theta_K)]$, and $\mathbf{s}(n) \triangleq [s_1(n), s_2(n), \dots, s_K(n)]^T$, $n = 1, \dots, N$, is the source waveform vector at time n .

The array steering matrix has different expressions, depending on the array geometry and on whether the source is in the near-field or far-field of the array. For instance, the steering vector corresponding to the k th source for a far-field linear array (where θ_k represents the impinging angle of source k in this case) is given by

$$\mathbf{a}(\theta_k) = [e^{-j(2\pi f/c_0)x_1 \cos(\theta_k)}, \dots, e^{-j(2\pi f/c_0)x_M \cos(\theta_k)}]^T \quad (2)$$

where f is the center frequency, c_0 is the wave propagation velocity, and x_m is the position of the m th sensor, $m = 1, \dots, M$. (See Fig. 1.) Note that for a planar array or near-field sources, only the expressions for the steering vectors have to be modified; the algorithms that are presented can be applied without any modifications, since $\mathbf{a}(\boldsymbol{\theta})$ is assumed to be a known function of $\boldsymbol{\theta}$. The number of sources, K , is usually unknown; hence, here, K is considered to be the number of scanning points in the region. In other words every point of a predefined grid that covers the region of interest is considered as a potential source whose power is estimated. Consequently,

¹With a slight abuse of notation, we do not use bold font for θ_k , $k = 1, \dots, K$, which might be multi-dimensional, for simplicity.

K will be much larger than the actual number of sources present, and only a few components of $\{\mathbf{s}(n)\}$ will be non-zero. This is the main reason why sparse algorithms can be used in array processing applications.

B. Related Work

We focus our attention on array processing algorithms exploiting sparsity, which have gained noticeable interest recently. Sparse signal representation aims at finding the sparsest \mathbf{s} , such that $\mathbf{y} = \mathbf{A}\mathbf{s}$ is satisfied, i.e., to minimize $\|\mathbf{s}\|_0$, such that $\mathbf{y} = \mathbf{A}\mathbf{s}$, where \mathbf{A} is known and \mathbf{y} is measured. The problem in its original form is a combinatorial problem and is nondeterministic polynomial-time (NP) hard, making it impractical [12]. Fortunately, when \mathbf{s} is sufficiently sparse [12–15], $\|\mathbf{s}\|_0$ can be replaced by $\|\mathbf{s}\|_1$, which leads to a convex optimization problem that can be solved much more easily by using, for instance, the least absolute shrinkage and selection operator (LASSO) [16] or basis pursuit (BP) [17] algorithms. Alternatively, the focal underdetermined system solution (FOCUSS) algorithm [18], which is derived using Lagrange multipliers, can be used to iteratively solve the sparse problem. A Bayesian approach, such as sparse Bayesian learning (SBL) [19, 20] or the approach in [21], can also be used to estimate \mathbf{s} . The algorithms mentioned up to this point are for the single-snapshot case only. The extensions of FOCUSS and SBL to the multiple-snapshot case are M-FOCUSS [22] and M-SBL [23], respectively. Another algorithm, the ℓ_1 -SVD (singular value decomposition) algorithm [24, 25] is similar to BP or LASSO, but this algorithm can work with multiple snapshots. (For the single-snapshot case, ℓ_1 -SVD becomes a LASSO and BP type of method.) M-FOCUSS requires the tuning of two hyperparameters, which might affect the performance of the algorithm significantly. ℓ_1 -SVD requires the tuning of a hyperparameter and an estimate for the number of sources. Moreover, implementing ℓ_1 -SVD requires convex optimization software, such as SeDuMi [44]. M-SBL does not require any hyperparameters. However, M-SBL converges quite slowly in its original form [19, 20, 23].

Besides the above algorithms, which are the focus of our attention in the numerical examples, there are other sparsity based approaches worth mentioning. Reference [26] adds an additional spatial sparsity regularizing term (an ℓ_2 -norm constraint) to the ℓ_1 -norm constraint, and it minimizes a cost function similar to that of ℓ_1 -SVD. However, this method has two hyperparameters, assumes that the source waveforms can be represented by a sparse basis, and has high computational complexity

[26]. Fuchs [27, 28] uses a sparsity-constrained deconvolution approach that assumes the sources are uncorrelated and that the number of snapshots is large. The sparsity-constrained solution is obtained with a LASSO or BP type of algorithm. Reference [29] introduces two hyperparameter free deconvolution algorithms exploiting sparsity: a sparsity-based extension to the deconvolution approach for the mapping of acoustic sources (DAMAS) [45] (which is similar to [27] and [28] and widely used in practice) and a sparsity based covariance-matrix fitting approach. Extensions to the correlated source case are also provided. However, the methods in [29] are based on the sample covariance matrix, and hence, these methods do not work well with a limited number of snapshots.

C. IAA-APES

IAA-APES is a data-dependent, nonparametric algorithm based on a weighted least squares (WLS) approach. Let \mathbf{P} be a $K \times K$ diagonal matrix, whose diagonal contains the power at each angle on the scanning grid. Then \mathbf{P} can be expressed as

$$P_k = \frac{1}{N} \sum_{n=1}^N |s_k(n)|^2, \quad k = 1, \dots, K. \quad (3)$$

Furthermore, define the interference (signals at angles other than the angle of current interest θ_k) and noise covariance matrix $\mathbf{Q}(\theta_k)$ to be

$$\mathbf{Q}(\theta_k) = \mathbf{R} - P_k \mathbf{a}(\theta_k) \mathbf{a}^H(\theta_k) \quad (4)$$

where $\mathbf{R} \triangleq \mathbf{A}(\theta) \mathbf{P} \mathbf{A}^H(\theta)$. Then the WLS cost function is given by (see, e.g., [34]–[36] and [43])

$$\sum_{n=1}^N \|\mathbf{y}(n) - s_k(n) \mathbf{a}(\theta_k)\|_{\mathbf{Q}^{-1}(\theta_k)}^2 \quad (5)$$

where $\|\mathbf{x}\|_{\mathbf{Q}^{-1}(\theta_k)}^2 \triangleq \mathbf{x}^H \mathbf{Q}^{-1}(\theta_k) \mathbf{x}$ and $s_k(n)$ represents the signal waveform at angle θ_k and at time n . Minimizing (5) with respect to $s_k(n)$, $n = 1, \dots, N$, yields

$$\hat{s}_k(n) = \frac{\mathbf{a}^H(\theta_k) \mathbf{Q}^{-1}(\theta_k) \mathbf{y}(n)}{\mathbf{a}^H(\theta_k) \mathbf{Q}^{-1}(\theta_k) \mathbf{a}(\theta_k)}, \quad n = 1, \dots, N. \quad (6)$$

This looks like the result that would be obtained by employing APES [34–36], but it is actually different than APES since APES obtains $\mathbf{Q}(\theta_k)$ from the data by forming subapertures, while IAA-APES computes $\mathbf{Q}(\theta_k)$, as in (4). Moreover, IAA-APES is iterative, but APES is not, and APES cannot be used with arbitrary array geometries.

Using (4) and the matrix inversion lemma, (6) can be written as

$$\hat{s}_k(n) = \frac{\mathbf{a}^H(\theta_k) \mathbf{R}^{-1} \mathbf{y}(n)}{\mathbf{a}^H(\theta_k) \mathbf{R}^{-1} \mathbf{a}(\theta_k)}, \quad n = 1, \dots, N. \quad (7)$$

TABLE II
The IAA-APES Algorithm

$$\hat{P}_k = \frac{1}{(\mathbf{a}^H(\theta_k)\mathbf{a}(\theta_k))^2 N} \sum_{n=1}^N |\mathbf{a}^H(\theta_k)\mathbf{y}(n)|^2, \quad k = 1, \dots, K$$

repeat
 $\mathbf{R} = \mathbf{A}(\theta)\hat{\mathbf{P}}\mathbf{A}^H(\theta)$
for $k = 1, \dots, K$
 $\hat{s}_k(n) = \frac{\mathbf{a}^H(\theta_k)\mathbf{R}^{-1}\mathbf{y}(n)}{\mathbf{a}^H(\theta_k)\mathbf{R}^{-1}\mathbf{a}(\theta_k)}, \quad n = 1, \dots, N$
 $\hat{P}_k = \frac{1}{N} \sum_{n=1}^N |\hat{s}_k(n)|^2$
end for
until (convergence)

TABLE III
The IAA-APES&BIC Algorithm

\mathcal{P} : Set of peaks obtained from IAA-APES
 $\mathcal{I} = \emptyset, \eta = 1, \text{quit} = 0, \text{BIC}^{\text{old}} = \infty$
repeat
 $i' = \arg \min_{i \in \mathcal{P} - \mathcal{I}} \text{BIC}_i(\eta)$
if $\text{BIC}_{i'}(\eta) < \text{BIC}^{\text{old}}$
 $\mathcal{I} = \{\mathcal{I}, i'\}$
 $\text{BIC}^{\text{old}} = \text{BIC}_{i'}(\eta)$
 $\eta = \eta + 1$
else $\text{quit} = 1$
until ($\text{quit} = 1$)

This avoids the computation of $\mathbf{Q}^{-1}(\theta_k)$ for each scanning point, i.e., K times. Moreover, $\{\hat{s}_k(n)\}$ can be computed in parallel for each scanning point, which makes IAA-APES amenable to implementation on parallel hardware. IAA-APES is summarized in Table II. Since IAA-APES requires \mathbf{R} , which itself depends on the unknown signal powers, it has to be implemented as an iteration. The initialization is done by a standard DAS beamformer. Our empirical experience is that IAA-APES does not provide significant improvements in performance after about 15 iterations. In IAA-APES, \mathbf{P} and, hence \mathbf{R} , are obtained from the signal estimates of the previous iteration and not from the snapshots as in conventional adaptive beamforming algorithms, such as SCB, which fails to work properly with coherent or highly correlated sources, or few snapshots [43]. The Appendix provides an alternative derivation of IAA-APES, based on the ML principle. IAA-APES is shown to be an approximation of the IAA-ML algorithm, which is locally convergent due to cyclically maximizing the likelihood function. Hence, the analysis in the Appendix provides an approximate calculation that shows the local convergence of IAA-APES.

Because \mathbf{P} is assumed to be a diagonal matrix, one degree of freedom (DOF) is needed to suppress one interfering source. This may lead to a larger

than necessary reduction of the number of degrees of freedom when some of the interfering sources are coherent since the cancellation of multiple coherent interfering sources would require only one DOF if the correct structure of \mathbf{P} were known. However, we do not assume that the true structure of \mathbf{P} is known. Moreover, it is the diagonal structure of \mathbf{P} assumed by IAA-APES that makes the algorithm work properly even for low number of snapshot cases and coherent sources.

D. IAA-APES&BIC

In many applications it is desirable to obtain point estimates rather than a continuous spatial estimate. To achieve this sparsity we incorporate a model-order selection tool, i.e., the BIC [37, 38], into IAA-APES. Let \mathcal{P} denote a set containing the indices of the peaks selected from the IAA-APES spatial power spectrum estimate. Also let \mathcal{I} denote the set of the indices of the peaks selected by the BIC algorithm so far. The IAA-APES&BIC algorithm works as follows: first the peak, from the set \mathcal{P} , giving the minimum BIC is selected. Then the second peak, from the set $\mathcal{P} - \mathcal{I}$, which together with the first peak gives the minimum BIC, is selected, and so on, until the BIC value does not decrease anymore.² The IAA-APES&BIC algorithm is summarized in Table III. $\text{BIC}_i(\eta)$ is calculated as follows (see [38])

$$\text{BIC}_i(\eta) = 2MN \ln \left(\sum_{n=1}^N \left\| \mathbf{y}(n) - \sum_{j \in \{\mathcal{I} \cup i\}} \mathbf{a}(\theta_j) \hat{\mathbf{s}}_j(n) \right\|_2^2 \right) + 3\eta \ln(2MN) \quad (8)$$

where $\eta = |\mathcal{I}| + 1$, $|\mathcal{I}|$ denotes the size of the set \mathcal{I} , i is the index of the current peak under consideration, and $\{\hat{\mathbf{s}}_j(n)\}_{n=1}^N$ is the IAA-APES signal waveform estimate corresponding to angle θ_j , $j \in \{\mathcal{I} \cup i\}$. Note that the second term on the right side of (8) does not matter to peak selection; it matters only when (8) is used to select the number of peaks to retain.

E. IAA-APES&RELAX

RELAX [39, 40] is a parametric cyclic algorithm that requires an estimate of the number of sources in the field. The results of IAA-APES&BIC can be used to provide a good initial estimate for the last step of RELAX. This approach is outlined in Table IV. The RELAX iterations can be terminated when the norm of the difference between two consecutive estimates is smaller than a certain threshold (5×10^{-4} for the examples considered herein). The maximization

²Alternatively, the largest η peaks can be selected so that when the $(\eta + 1)$ st largest peak is added to \mathcal{I} , the BIC value does not decrease. This simplified version gives similar results to the one described above in our numerical examples.

TABLE IV
The IAA-APES&RELAX Algorithm

θ' : Locations of the peaks obtained from IAA-APES&BIC
 K' : Number of peaks obtained from IAA-APES&BIC
 $\{\hat{s}_k(n)\}$: Corresponding waveforms obtained from IAA-APES&BIC
repeat
 for $k = 1, \dots, K'$
 $\mathbf{y}_k(n) = \mathbf{y}(n) - \sum_{\substack{l=1 \\ l \neq k}}^{K'} \mathbf{a}(\theta'_l) \hat{s}_l(n), \quad n = 1, \dots, N$
 $\hat{\theta}'_k = \arg \max_{\theta' \in \mathbb{R}} \sum_{n=1}^N |\mathbf{a}^H(\theta') \mathbf{y}_k(n)|^2$
 $\hat{s}_k(n) = \frac{1}{M} \mathbf{a}^H(\hat{\theta}'_k) \mathbf{y}_k(n), \quad n = 1, \dots, N$
 end for
until (convergence)

step of the algorithm can be implemented without much computational effort by means of a fine search only around the peak values of the IAA-APES&BIC result.³ RELAX can be useful in estimating off-grid sources accurately and for further improving the IAA-APES waveform and angle estimates.

III. ACTIVE SENSING

In active sensing applications, besides the receiver, there are also one or more transmitters. The radar/sonar range-Doppler imaging problem for a SISO system is first investigated in this section. Then the channel estimation problem for MISO communications is discussed.

A. Range-Doppler Imaging

Pulse compression refers to the process of transmitting a modulated pulse and then matched filtering the returned signal, which arrives at the antenna altered by complex coefficients that bear target information [48].

1) *Data Model*: Consider a range-Doppler imaging radar/sonar with a transmitted pulse

$$\tilde{\mathbf{s}} = [\tilde{s}(1), \tilde{s}(2), \dots, \tilde{s}(M)]^T \quad (9)$$

where M is the pulse length. Let

$$\mathbf{s}(\omega_l) = \tilde{\mathbf{s}} \odot \mathbf{d}(\omega_l) \quad (10)$$

be the Doppler shifted signal, where

$$\mathbf{d}(\omega_l) = [1, e^{j\omega_l}, \dots, e^{j(M-1)\omega_l}]^T, \quad l = 1, \dots, L \quad (11)$$

³The fine search can be implemented efficiently using the fast Fourier transform (FFT) [39, 40] or a derivative-free uphill search method, such as the Nelder-Mead algorithm [46, 47]. Note that the latter method is available in the MATLAB optimization toolbox with the name of “fminsearch.”

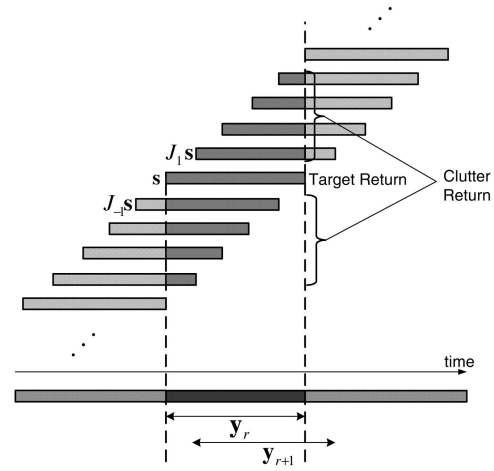


Fig. 2. Pulse compression for radar/sonar range-Doppler imaging.

the Doppler interval of interest is divided into L bins, and the Doppler frequency for the l th Doppler bin is denoted as ω_l . Then the M samples of the received signal that is temporally aligned with the return from the range bin of current interest r (see Fig. 2) can be represented by

$$\mathbf{y}_r = \sum_{l=1}^L \alpha_{r,l} \mathbf{s}(\omega_l) + \sum_{\substack{m=-M+1 \\ m \neq 0}}^{M-1} \sum_{l=1}^L \alpha_{r+m,l} \mathbf{J}_m \mathbf{s}(\omega_l) + \mathbf{e}_r \quad (12)$$

for $r = 1, \dots, R$, where $\alpha_{r,l}$ (which is proportional to the complex “voltage” radar-cross section (RCS) of the corresponding target) denotes the complex amplitude of the returned signal from the range bin of current interest r and the l th Doppler bin $\{\alpha_{m+r,l}\}$ denote the complex amplitudes of the returned signals from the adjacent range bins, and \mathbf{e}_r denotes the noise. The reflections from nearby range bins are considered to be clutter. The $M \times M$ shift matrix \mathbf{J}_m takes into account the fact that the clutter returns from adjacent range bins need different propagation times to reach the radar/sonar receiver:

$$\mathbf{J}_m = \begin{bmatrix} \leftarrow & m & \rightarrow \\ 0 & \dots & 1 & \dots & 0 \\ \vdots & \ddots & & \ddots & \vdots \\ 0 & & \ddots & & 1 \\ \vdots & \ddots & & \ddots & \vdots \\ 0 & \dots & 0 & \dots & 0 \end{bmatrix} = \mathbf{J}_{-m}^T \quad (13)$$

for $m = 0, \dots, M-1$. Equation (12) can be written as

$$\mathbf{y}_r = \mathbf{S} \boldsymbol{\alpha}_r + \tilde{\mathbf{e}}_r \quad (14)$$

where

$$\mathbf{S} = [\mathbf{s}(\omega_1), \mathbf{s}(\omega_2), \dots, \mathbf{s}(\omega_L)] \quad (15)$$

$$\boldsymbol{\alpha}_r = [\alpha_{r,1}, \alpha_{r,2}, \dots, \alpha_{r,L}]^T \quad (16)$$

and

$$\tilde{\mathbf{e}}_r = \sum_{\substack{m=-M+1 \\ m \neq 0}}^{M-1} \sum_{l=1}^L \alpha_{r+m,l} \mathbf{J}_m \mathbf{s}(\omega_l) + \mathbf{e}_r. \quad (17)$$

Note that (12) is similar to the data model for passive sensing arrays, see (1), but with a single snapshot. The IAA-APES estimate at iteration number $i \in \{1, 2, \dots\}$ becomes

$$\hat{\alpha}_{r,l}^{(i)} = \frac{\mathbf{s}^H(\omega_l) \mathbf{R}_{(i-1)}^{-1}(r) \mathbf{y}_r}{\mathbf{s}^H(\omega_l) \mathbf{R}_{(i-1)}^{-1}(r) \mathbf{s}(\omega_l)} \quad (18)$$

for $l = 1, \dots, L$, $r = 1, \dots, R$, where

$$\mathbf{R}_{(i-1)}(r) = \sum_{m=-M+1}^{M-1} \sum_{l=1}^L |\hat{\alpha}_{r+m,l}^{(i-1)}|^2 \mathbf{J}_m \mathbf{s}(\omega_l) \mathbf{s}^H(\omega_l) \mathbf{J}_m^T. \quad (19)$$

Here IAA-APES is applied in a slightly different manner than in the passive array processing case. When α_r is to be estimated, the previous values of $\{\alpha_{r+m}\}_{m=-M+1}^{M-1}$ are used to estimate $\mathbf{R}(r)$. However, only α_r is updated using $\mathbf{R}(r)$ and \mathbf{y}_r . When all $\{\alpha_r\}_{r=1}^R$ are updated in this way, we advance to the next IAA-APES iteration. IAA-APES is initialized by matched filtering, matched to each range and Doppler bin, to obtain the initial $\{\alpha_{r,l}\}$.

2) *Related Work*: Matched filtering has been widely used for pulse compression because it gives optimal signal-power-to-output-power performance in the presence of a single target and white noise. However, in practical radar/sonar systems, matched filter performance is far from desirable since the pulse compression problem is usually clutter limited rather than noise limited (see, e.g., [49] and [50]). Many data independent (see, e.g., [49]–[54]) and data-adaptive (see, e.g., [48] and [55]) approaches have been proposed to achieve improved pulse compression.

Data independent approaches can be designed off-line, and hence, these approaches are convenient for real-time implementations in practical systems. Although receive filters based on data-independent instrumental variables (IV) can be used to achieve excellent pulse compression for the negligible Doppler case, their performance is unsatisfactory in the nonnegligible Doppler case because of high sidelobe level problems [49]. On the other hand data-adaptive approaches result in better performance but at the cost of implementation complexity. Two important data-adaptive methods for pulse compression are the adaptive pulse compression (APC) [48] and the Doppler-compensated APC (DC-APC) [55] algorithms. APC is an iterative minimum mean-squared error (MMSE) based data adaptive approach, and DC-APC is the extension of APC to the nonnegligible Doppler case. However, an IV approach [49] may be preferred to APC since the sidelobe level of the former method can be made arbitrarily low and because the filter coefficients

can be computed off-line, whereas APC updates the filter coefficients iteratively and adaptively. In the nonnegligible Doppler case, however, adaptive approaches can perform much better. DC-APC is purported to work with at most one target per range bin, and the method used in [55] to estimate the Doppler values is not appealing from a performance viewpoint. On the other hand, IAA-APES can work with multiple Doppler targets located at the same range bin, and IAA-APES estimates the Doppler values in a robust manner. Moreover, APC and DC-APC require the tuning of hyperparameters, whereas IAA-APES is hyperparameter free. Some other differences are discussed below.

DC-APC assumes that there is at most one target per range bin. Let $\{\alpha_{r-M+1}, \dots, \alpha_{r+M-1}\}$ and $\{\tilde{\omega}_{r-M+1}, \dots, \tilde{\omega}_{r+M-1}\}$ denote the complex amplitudes and the Doppler frequencies, respectively, of the targets in the corresponding range bin r . DC-APC estimates the target parameters iteratively as follows

$$\alpha_r^{(i)} = |\alpha_r^{(i-1)}|^2 \mathbf{s}^H(\tilde{\omega}_r) \mathbf{R}_{(i-1)}^{-1}(r) \mathbf{y}_r \quad (20)$$

for $r = 1, \dots, R$, where

$$\mathbf{R}_{(i-1)}(r) = \sum_{m=-M+1}^{M-1} |\alpha_{r+m}^{(i-1)}|^2 \mathbf{J}_m \mathbf{s}(\tilde{\omega}_{r+m}) \mathbf{s}^H(\tilde{\omega}_{r+m}) \mathbf{J}_m^T + \mathbf{Q}_r. \quad (21)$$

\mathbf{Q}_r is the true noise covariance matrix of \mathbf{e}_r , which is assumed to be known, and $i \in \{1, 2, \dots\}$ represents the current iteration number. The initial estimates of $\{\alpha_{r+m}\}_{m=-M+1}^{M-1}$ are obtained by using a standard matched filter that neglects the Doppler effect [55]. DC-APC also requires the estimates $\{\tilde{\omega}_{r+m}\}_{m=-M+1}^{M-1}$ of the target Doppler frequencies at each iteration. The Doppler frequency estimation approaches suggested in [55] are ad-hoc and not very accurate, especially for large Doppler shifts. This limitation of DC-APC, though, can be easily corrected by replacing $\tilde{\omega}_r$ in (20) with all possible Doppler frequencies $\{\omega_l\}$ to deal with multiple targets per range bin and to form range-Doppler images.

The DC-APC iterations defined in (20)–(21) result in the numerical ill-conditioning of $\mathbf{R}_{(i-1)}(r)$. To mitigate this problem, [48] suggests using $|\alpha_r^{(i-1)}|^\delta$ in (20) instead of $|\alpha_r^{(i-1)}|^2$, and σ^δ instead of σ^2 , where $0 \leq \delta \leq 2$ and where the noise \mathbf{e}_r is assumed to be white with a known variance σ^2 . This approach requires the delicate tuning of δ (at each iteration), but [48] and [55] do not provide a clear guideline on how to do this. We remark that if the noise covariance matrix \mathbf{Q}_r in (21) is set to zero, then APC/DC-APC becomes identical to FOCUSS, with the sparsity parameter $p = 0$ and the regularization parameter $\lambda = 0$. (See, e.g., (16) in [22]). In addition, with the introduction of δ , APC/DC-APC is still identical to FOCUSS, now with $1 - p/2 = \delta/2$ and $\lambda = \sigma^\delta$. We

also note that both APC/DC-APC and FOCUSS are related to the approaches in [21], [30], and [56]. It is interesting to note that many different ideas lead to the same result.

IAA-APES assumes that multiple targets can exist within the same range bin and that $\{\alpha_{r,l}\}$ is calculated as in (18), where the term in the denominator can be viewed as the current estimate of $|\alpha_r^{(i-1)}|^2$ used in (20). This would be best estimate for $|\alpha_r^{(i-1)}|^2$, obtained by applying the minimum variance distortionless criterion, had the true covariance matrix been known [5]. One more advantage of IAA-APES is that the parameter estimates are inherently unbiased for the signal of interest, whereas this is not the case in DC-APC (or FOCUSS). Furthermore, in IAA-APES, the statistical properties of \mathbf{e}_r are assumed unknown and are taken into account implicitly as false targets in the current and adjacent range and Doppler bins; see (19). No matrix inversion problems were encountered with IAA-APES during our numerical simulations because of the unbiasedness property of IAA-APES.

B. Channel Estimation

The purpose of channel estimation in communications is to provide the subsequent equalizer with an accurate channel estimate so that the transmitted signals can be recovered successfully at the receiver side [57, 58]. SISO channel estimation for communications problem is similar to SISO radar/sonar range-Doppler imaging, with the only difference being that the delay for the former is due to single-trip propagation, while the delay for the latter results from round-trip propagation.

1) *Data Model*: For the MISO channel estimation problem with I transmitters and a single receiver, let

$$\tilde{\mathbf{s}}_i = [\tilde{s}_i(1), \tilde{s}_i(2), \dots, \tilde{s}_i(M)]^T, \quad i = 1, \dots, I \quad (22)$$

denote the i th transmitted pulse, and let L denote the total number of Doppler bins. Then similar to (12), the received signal that is temporally aligned with the return from the r th tap, $r = 1, \dots, R$, with R denoting the total number of taps of the channel, can be written as

$$\mathbf{y}_r = \sum_{i=1}^I \left\{ \sum_{l=1}^L \alpha_{r,l}(i) \mathbf{s}_i(\omega_l) + \sum_{\substack{m=-M+1 \\ m \neq 0}}^{M-1} \sum_{l=1}^L \alpha_{r+m,l}(i) \mathbf{J}_m \mathbf{s}_i(\omega_l) \right\} + \mathbf{e}_r \quad (23)$$

where \mathbf{J}_m was defined in (13),

$$\mathbf{s}_i(\omega_l) = \tilde{\mathbf{s}}_i \odot \mathbf{d}(\omega_l) \quad (24)$$

and $\mathbf{d}(\omega_l)$ was defined in (11). When determining the parameters of the i th channel $\{\alpha_{r,l}(i)\}$, the term $\sum_{l=1}^L \alpha_{r,l}(i) \mathbf{s}_i(\omega_l)$ is the signal term, and all other terms in (23) are considered as clutter and noise.

Consequently, IAA-APES can be applied directly to (23) to estimate $\{\alpha_{r,l}(i)\}$. Like in radar/sonar range compression problems, to determine $\{\alpha_{r,l}(i)\}$ with high accuracy, the transmitted pulses need to have both good auto and cross-correlation properties [59, 60].

2) *Related Work*: Most of the demodulation algorithms used in practice rely heavily on the accurate estimation of the channel impulse response. As in many other applications, sparse signal estimation approaches have also been proposed in this context. The main motivation for this is that underwater communications [61–63] and wireless channels are appropriately modelled as sparse channels consisting of only a few non-zero taps [64]. The existing approaches we evaluate for sparse channel estimation, besides IAA-APES, include the matching pursuit (MP), orthogonal matching pursuit (OMP) [65–67], and least squares matching pursuit (LSMP) [68] algorithms, which have been used for sparse channel estimation and equalization in many applications [69–72]. It is difficult to determine the stopping criterion when using matching pursuit algorithms, and user intervention is needed.

IV. NUMERICAL EXAMPLES

We evaluate the performance of IAA-APES and compare it with various alternative methods in this section. We first focus on passive sensing applications and then shift our attention to active sensing applications.

A. Passive Sensing Examples

This subsection investigates the performance of IAA-APES, M-FOCUSS, M-SBL and ℓ_1 -SVD for various passive sensing scenarios. Unless noted otherwise, M-FOCUSS is implemented by setting the sparsity parameter $p = 0.8$ and fine tuning the regularization parameter λ to get the best results.⁴ ℓ_1 -SVD is implemented by assuming that the number of sources is known a priori and by fine tuning the hyperparameter. Since the fine tuning of the hyperparameters assume knowledge of the true source parameters, the so obtained results of M-FOCUSS and ℓ_1 -SVD are impractical. M-SBL is implemented by using the alternative update method for the parameters as described in [19], [20], and [23]. For all approaches considered, the scanning grid is uniform in the range from 1° to 180° , with 1° increment between adjacent grid points, unless noted otherwise.

We consider a uniform linear array with $M = 12$ sensors and half-wavelength interelement spacing.

⁴See Section VE in [22]. Also note that the M-FOCUSS algorithm used here is referred to as regularized M-FOCUSS in [22] since $\lambda \neq 0$. We refer to the approach as M-FOCUSS for simplicity.

The far-field narrowband signal waveforms and the additive noise signals are assumed to be circularly symmetric, independent identically distributed (i.i.d.) complex Gaussian random processes with zero mean and variance σ^2 , which is varied to obtain various SNR values. Furthermore, each signal waveform is normalized such that $(1/N) \sum_{n=1}^N |s_k(n)|^2 = P_k$, $k = 1, \dots, K_0$, for a given P_k value, where K_0 denotes the true number of sources. SNR is defined as $10 \log_{10}(P_k/\sigma^2)$, $k = 1, \dots, K_0$, in decibels (dB), where σ^2 is the noise variance. According to the comments made in the Introduction, we consider very low snapshot cases, viz. $N = 3$ and $N = 1$.

First we consider three uncorrelated sources at 60° , 82° , and 90° , with 5 dB, 10 dB, and 10 dB powers, respectively, and with $N = 3$. The noise power is 0 dB, which results in a minimum SNR of 5 dB. Fig. 3 shows the power and location estimates of the algorithms. The circles and the vertical dotted lines that align with these circles represent the true source locations and powers, and the results of 10 Monte-Carlo trials are shown in each plot. DAS clearly suffers from smearing and leakage. IAA-APES provides a much better result than DAS, with low sidelobes and peaks at the true source locations. Moreover, IAA-APES&RELAX indicates the number of sources and their locations and powers accurately. As observed in Fig. 3(d)–(f), the sparse algorithms encounter source splitting, location bias, and power underestimation problems. Also it is hard to tell how many sources are present by solely using the spatial estimates of the sparse algorithms.

Next Fig. 4 considers three coherent sources at 60° , 80° , and 90° , with 10 dB power each and with $N = 3$. The source waveforms are assumed to be identical for all three coherent sources. The noise power is 0 dB, resulting in a 10 dB SNR. Similar to Fig. 3, the circles and the vertical dotted lines represent the true source locations and the powers, and the results of 10 Monte-Carlo trials are shown in each plot. We observe that IAA-APES is able to resolve the sources successfully and that IAA-APES&RELAX provides accurate point estimates. On the other hand DAS fails to resolve the two closely spaced sources. The performances of the sparse algorithms are similar to those of the previous example.

Finally Fig. 5(a) compares the total mean-squared error (MSE) (sum of each individual MSE) of the angle estimates of each algorithm with the Cramer-Rao bound (CRB) [5], and Fig. 5(b) compares the total angle estimation bias (sum of each individual bias' modulus) of each algorithm for varying SNR. Two uncorrelated sources are placed at 77.51° and 90.51° , and N is set to 1. (The angle values are picked so that they are not on the size 1° grid used by IAA-APES.) To calculate the MSE and bias, we consider only the signals with the two largest powers

as the estimated signals for FOCUSS and ℓ_1 -SVD. We run the sparse algorithms, with a fine grid of size 0.01° , around the true source locations. The sparse algorithms are run with $K = 950$ scanning points, whereas IAA-APES is run with the same resolution as before, i.e., $K = 180$. IAA-APES&RELAX is used to estimate the off-grid sources. M-SBL results are not shown because of the excessive computation time needed. Each point in Fig. 5 is the average of 100 Monte-Carlo trials. We observe that IAA-APES&RELAX has both better variance and bias characteristics than the other methods for lower SNR.

Note that FOCUSS and ℓ_1 -SVD both have two hyperparameters, and their selection affects the performances of these two algorithms significantly. Moreover, a different parameter setting should be used depending on the SNR, N , and the source structure, i.e., the number of sources, source spacing, source power levels, and correlation levels. We were able to tune the parameters relatively easily in our simulation scenarios, but when the problem dimensions are large and when there is no prior knowledge of the scenario, it becomes difficult to find good hyperparameters. M-SBL, on the other hand, does not require any hyperparameters, but it takes the longest time to converge. These are the main reasons why BP or LASSO, which are the single-snapshot counterpart of ℓ_1 -SVD, and SBL and FOCUSS, which are the single snapshot counterparts of M-FOCUSS and M-SBL, are not considered in the active sensing examples below.

Assuming $K \gg M$, the complexity of each IAA-APES iteration is $\mathcal{O}(M^2K)$. The complexity of the BIC extension is negligible compared to that of IAA-APES, and the complexity of the RELAX extension depends on how many sources IAA-APES&BIC determines, the termination condition, and the method chosen for the maximization step. In our experiments RELAX usually converged faster than the time needed for IAA-APES to converge. The complexities of M-FOCUSS and M-SBL are also $\mathcal{O}(M^2K)$ per iteration [23]. The complexity of ℓ_1 -SVD, on the other hand, is $\mathcal{O}(K^3K_{\text{svd}}^3)$ [25], where K_{svd} is the estimate of the number of sources. In our simulations IAA-APES was always faster than M-FOCUSS, M-SBL, and ℓ_1 -SVD, especially when the SNR was low. Note that the actual number of iterations required for convergence depends heavily on the specific scenario. For example for the scenario considered in Fig. 5 at SNR = 2 dB, the times required by FOCUSS and ℓ_1 -SVD are 3.9 and 5.6 s, respectively, whereas IAA-APES&RELAX requires 0.1 s on average.⁵

⁵The timing values in seconds are given as an example. The convergence times may vary depending on many factors such as how the algorithms are implemented, the specific hardware, etc. ℓ_1 -SVD has been implemented using the software described in [73] and [44].

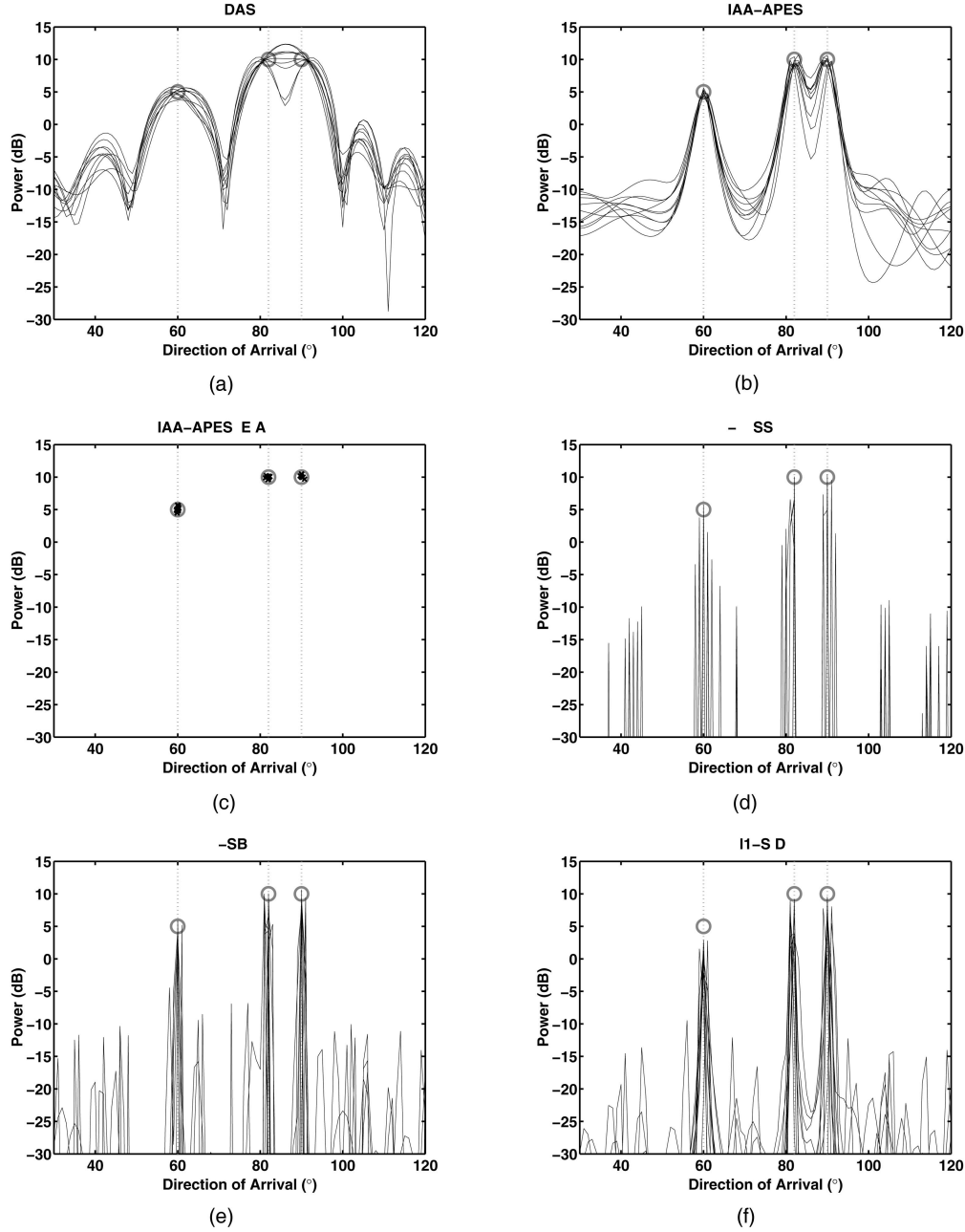


Fig. 3. Three uncorrelated sources at 60° (5 dB power), 82° (10 dB power), and 90° (10 dB power), as represented by circles and vertical dotted lines in each plot. $N = 3$, the noise power is 0 dB (which results in minimum SNR of 5 dB), and 10 Monte-Carlo trials are shown. (a) DAS spatial estimate. (b) IAA-APES spatial estimate. (c) IAA-APES&RELAX point source estimates. (d) M-FOCUSS spatial estimate. (e) M-SBL spatial estimate. (f) ℓ_1 -SVD spatial estimate.

B. Active Sensing Examples

This section considers examples for the SISO radar/sonar and the MISO channel estimation problems.

1) *SISO Range-Doppler Imaging Example:* We now evaluate the performance of IAA-APES for SISO range-Doppler imaging and compare it with that of the matched filtering, MP, OMP, and LSMP. We use a 30-element P3 code for the transmitted pulse, i.e., $\tilde{s}(m) = e^{j(m-1)^2\pi/M}$, and $m = 1, \dots, M$, where $M = 30$ [55, 74]. The Doppler shift is expressed as

$\Phi_l = \omega_l M(180^\circ/\pi)$, $l = 1, \dots, L$, which is the total phase shift (in degrees) for the transmitted pulse duration.

We consider three moving targets with 5 dB power and with Doppler shifts of -30° , -25° , and 15° and six moving targets with 25 dB power and Doppler shifts of -70° , -55° , -10° , 10° , 20° , and 60° , as shown in Fig. 6(a). The background noise is assumed to be a circularly symmetric i.i.d. complex Gaussian random process, with mean zero and a variance of 0 dB. The number of range bins is set to 100, and the number of Doppler bins is set to

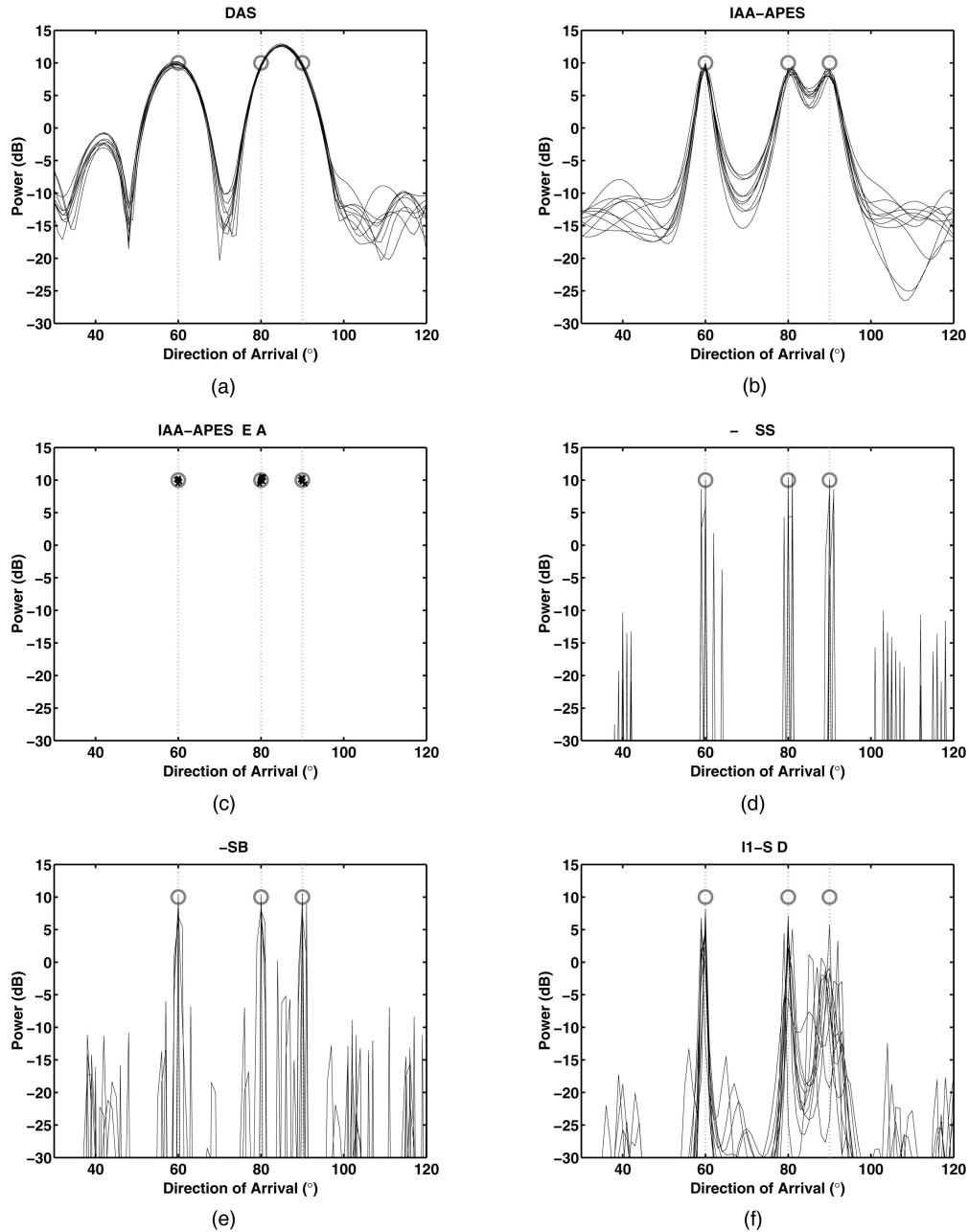


Fig. 4. Three coherent sources at 60° , 80° , and 90° , each with 10 dB power, as represented by circles and vertical dotted lines in each plot. $N = 3$, noise power is 0 dB (SNR = 10 dB), and 10 Monte-Carlo trials are shown. (a) DAS spatial estimate. (b) IAA-APES spatial estimate. (c) IAA-APES&RELAX point source estimates. (d) M-FOCUSS spatial estimate. (e) M-SBL spatial estimate. (f) ℓ_1 -SVD spatial estimate.

37. The resulting minimum SNR is 5 dB. Fig. 6 shows that the matched filter smears the targets in both the Doppler and range domains significantly. Figs. 6(c)–(e) show that MP, OMP, and LSMP results are not satisfactory in this example. The MP, OMP, and LSMP algorithms are all terminated manually to give the best performance.⁶ Fig. 6(f) shows that IAA-APES provides a much more useful result (the

⁶See [70] for a complexity analysis of MP, OMP, and LSMP. In our examples MP and OMP took less time than IAA-APES, whereas LSMP took longer than IAA-APES to converge.

target locations and Doppler frequencies being easily observable) than the matched filter. IAA-APES&BIC can estimate the strong targets accurately and the weak targets reasonably well, as shown in Fig. 6(g). IAA-APES&RELAX helps improve the results of IAA-APES&BIC even further, as shown in Fig. 6(h). In Figs. 6(c)–(e) and Figs. 6(g)–(h), the cross marks represent the targets selected by the algorithms, and the circles represent the ground truth. The numbers shown in Figs. 6(g)–(h) are the power estimates obtained by the corresponding algorithms. Recall that BIC selects only the dominant components of the

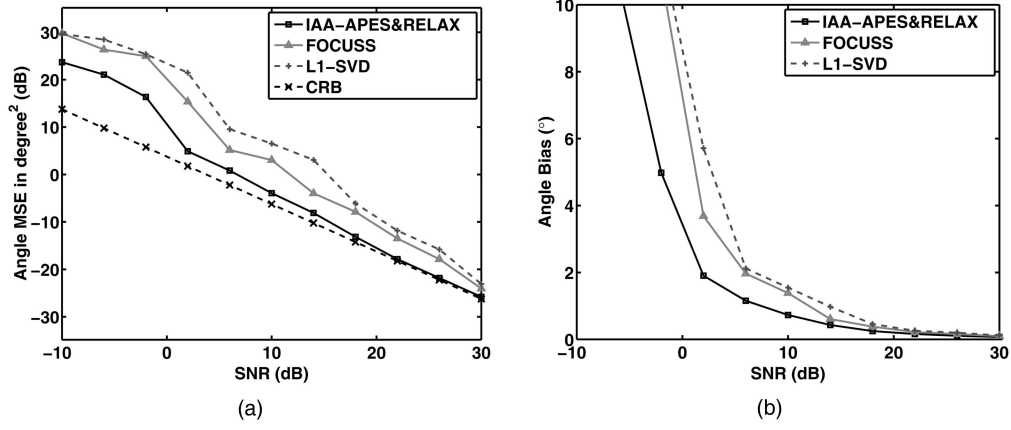


Fig. 5. Two uncorrelated sources at 77.51° and 90.51° with $N = 1$. (a) Total angle estimation MSE in dB together with CRB. (b) Total angle estimation bias versus SNR. Each point is average of 100 Monte-Carlo trials. Recall that FOCUSS is single snapshot version of M-FOCUSS.

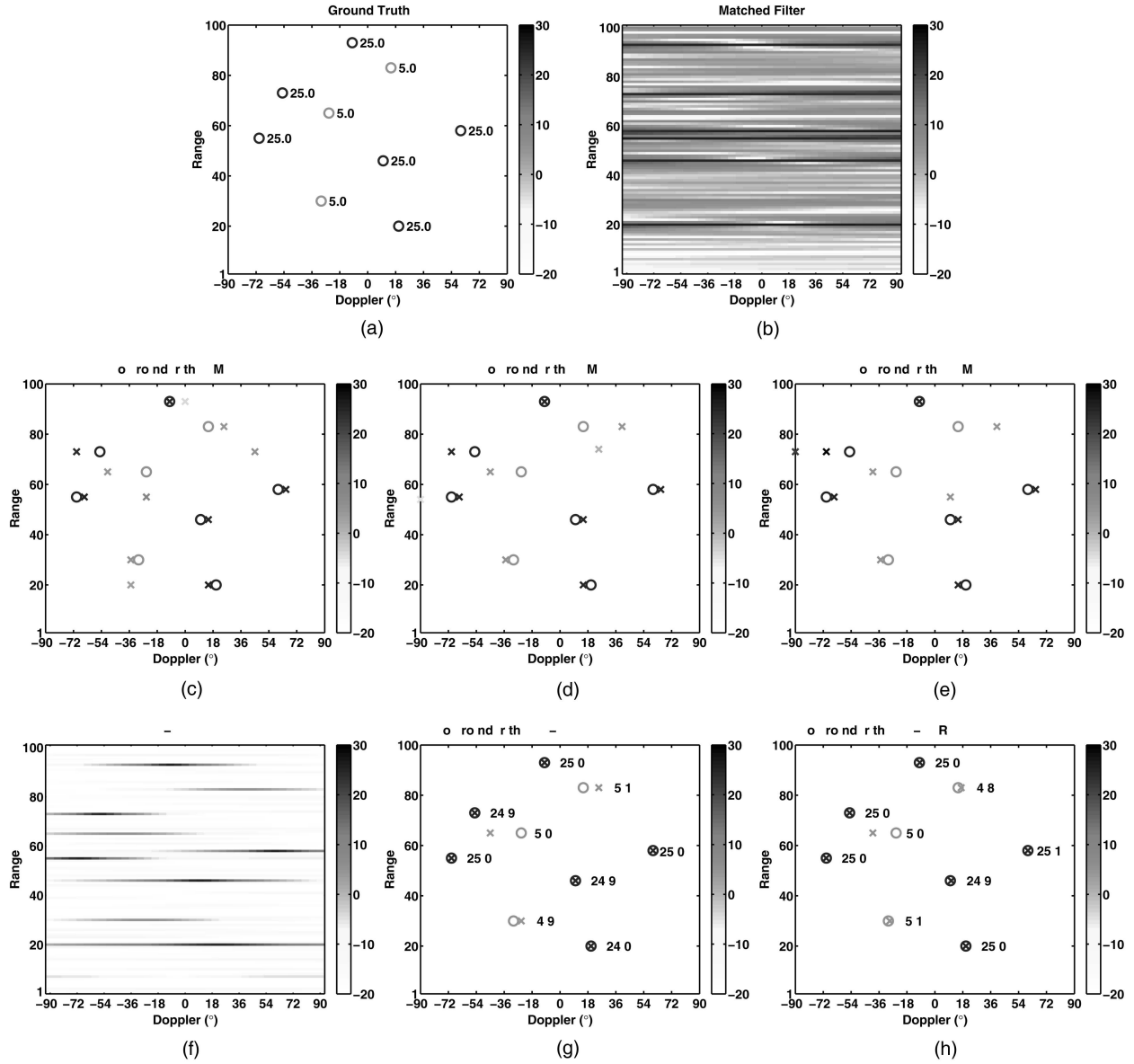


Fig. 6. SISO range-Doppler imaging with three 5 dB and six 25 dB targets, indicated by circles. Noise power is 0 dB, resulting in minimum SNR of 5 dB. (a) Ground truth with power levels. (b) Matched filter. (c) MP and ground truth. (d) OMP and ground truth. (e) LSMP and ground truth. (f) IAA-APES. (g) IAA-APES&BIC and ground truth. (h) IAA-APES&RELAX and ground truth. All power levels are in dB.

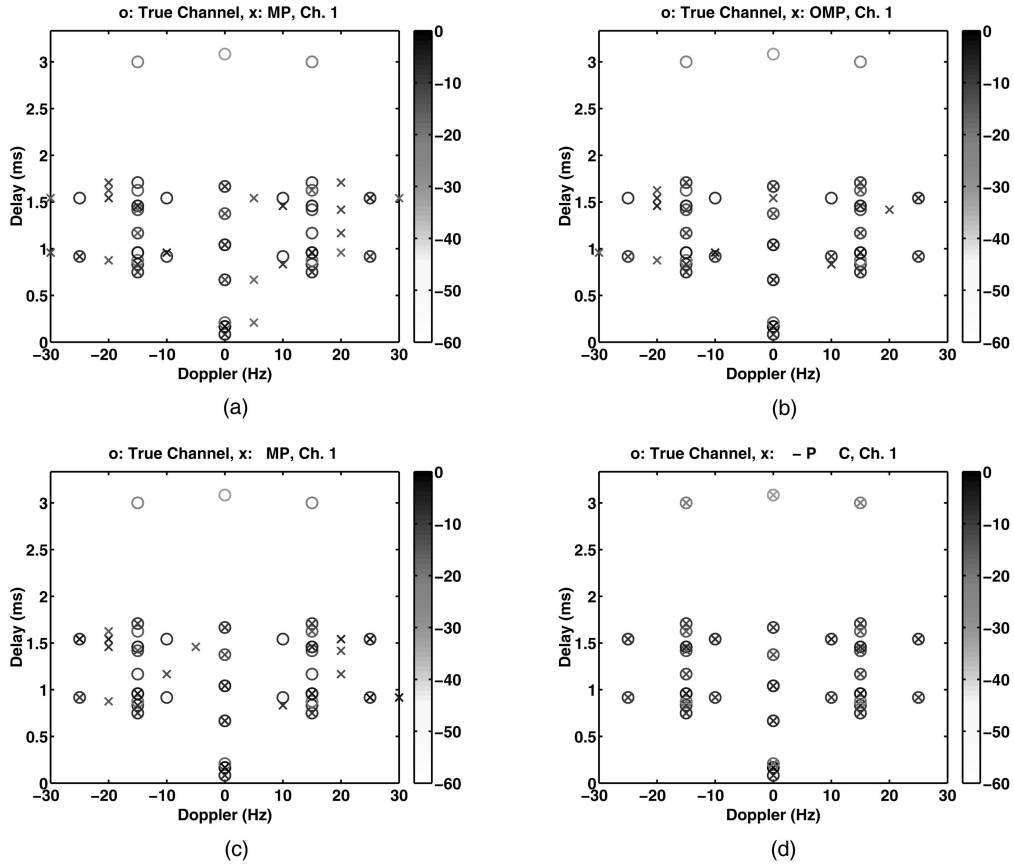


Fig. 7. MISO channel estimation with six transmitters and one receiver. Channel taps are indicated by circles. Channel tap power levels are in range of -30 dB to 0 dB, and noise level is -20 dB, which results in -10 dB minimum SNR. Estimates for first channel via (a) MP, (b) OMP, (c) LSMP, and (d) IAA-APES&BIC. All power levels are in dB.

IAA-APES spatial estimate, but BIC does not modify either the range-Doppler values or the power levels estimated by IAA-APES, whereas RELAX improves upon the IAA-APES estimates.

2) *Channel Estimation*: The performance of MP, OMP, LSMP, and IAA-APES are also investigated for the channel estimation problem encountered in communications. We consider six transmitters, viz. $I = 6$, and a single receiver. The probing pulses used in the simulations are obtained by using a cyclic algorithm to ensure both good auto and cross-correlation properties; see [59] and [60] for details. The sampling frequency is assumed to be 24 kHz. M is chosen to be 1024 (which yields a 42.7 ms pulse duration). The number of delay taps are set at 80 to yield a 3.3 ms of delay span, and 13 Doppler bins are used to cover the range from -30 Hz to 30 Hz with 5° resolution. The six channels are assumed to be independent of each other, and they are simulated as circularly symmetric i.i.d. complex Gaussian random variables, with mean zero and a variance decreasing exponentially with increasing delay, specifically $\sigma_k^2 = e^{-0.03(k-1)}$, where σ_k^2 is the variance of the channel tap with delay index k , $k = 1, \dots, 80$. The noise is simulated as a circularly symmetric i.i.d. complex Gaussian random process,

with mean zero and a -20 dB variance. The locations of the non-zero taps of the channels are also simulated randomly and by trying to mimic practical channel functions encountered in underwater communications, see, e.g., [69] and [70]. The power levels of the channel taps were in the range from -30 dB to 0 dB, which results in a minimum SNR of -10 dB. Fig. 7 illustrates the performances of the algorithms for the first channel; IAA-APES&BIC provides the best result. The results for the other channels, which are not shown for conciseness, are similar to that for the first channel.

V. CONCLUSIONS

This paper has presented IAA-APES in array processing applications. IAA-APES is a nonparametric, hyperparameter free algorithm that is designed to work under severe snapshot limitations and for uncorrelated, partially correlated, and coherent sources, as well as for arrays with arbitrary geometries. Because of the similarities between many active sensing applications and passive array processing, IAA-APES can be applied to these cases as well, without any essential modifications. The BIC can be used in conjunction with the IAA-APES

algorithm to yield sparse solutions, which are desirable in many applications. Furthermore, the application of the parametric RELAX algorithm to the IAA-APES&BIC results provides further performance improvement. Simulations showed that IAA-APES and its variations outperform the most prominent methods in the literature in the corresponding application areas. IAA-APES is believed to be a viable candidate for practical applications since it does not require any hyperparameters, has a simple formulation, provides superresolution, facilitates parallel processing, and shows good performance.

APPENDIX. AN APPROXIMATE ML INTERPRETATION OF IAA-APES

We derive a locally convergent ML-based iterative adaptive approach called IAA-ML. IAA-ML is similar to IAA-APES in nature, and we show that IAA-APES can be obtained as a simplified version of IAA-ML.

The negative log-likelihood function of $\{\mathbf{y}(n)\}_{n=1}^N$ can be represented as

$$\ln|\mathbf{R}| + \text{tr}(\mathbf{R}^{-1}\mathbf{\Gamma}) \quad (25)$$

where $\mathbf{\Gamma} = (1/N) \sum_{n=1}^N \mathbf{y}(n)\mathbf{y}^H(n)$ is the so-called sample covariance matrix. It is assumed that the received signal is a multivariate, complex Gaussian random vector with zero-mean and covariance matrix \mathbf{R} and that the snapshots are i.i.d. [5]. Minimizing (25) is equivalent to minimizing the Stein's loss, $-\ln|\mathbf{R}^{-1}\mathbf{\Gamma}| + \text{tr}(\mathbf{R}^{-1}\mathbf{\Gamma})$ [75, 76], which stresses the covariance fitting character of the cost function, but without the i.i.d. Gaussian assumptions needed by the maximum likelihood loss function.

Assume that $\mathbf{Q}(\theta_k)$ is known and that the signal power at θ_k is to be estimated. Using the fact that $|\mathbf{I} + \mathbf{A}\mathbf{B}| = |\mathbf{I} + \mathbf{B}\mathbf{A}|$ and the matrix inversion lemma together with (4), it can be shown that minimizing (25), with respect to P_k , is equivalent to minimizing

$$f(P_k) \triangleq \ln(1 + P_k \mathbf{a}_k^H \mathbf{Q}_k^{-1} \mathbf{a}_k) - \frac{P_k \mathbf{a}_k^H \mathbf{Q}_k^{-1} \mathbf{\Gamma} \mathbf{Q}_k^{-1} \mathbf{a}_k}{1 + P_k \mathbf{a}_k^H \mathbf{Q}_k^{-1} \mathbf{a}_k} \quad (26)$$

where $\mathbf{Q}(\theta_k)$ and $\mathbf{a}(\theta_k)$ have been replaced by \mathbf{Q}_k and \mathbf{a}_k , respectively, for notational simplicity. Setting the first derivative of (26), with respect to P_k , to zero, i.e., $f'(\tilde{P}_k) = 0$, gives

$$\tilde{P}_k = \frac{\mathbf{a}_k^H \mathbf{Q}_k^{-1} (\mathbf{\Gamma} - \mathbf{Q}_k) \mathbf{Q}_k^{-1} \mathbf{a}_k}{(\mathbf{a}_k^H \mathbf{Q}_k^{-1} \mathbf{a}_k)^2}. \quad (27)$$

The second derivative of (26), with respect to P_k , is

$$f''(P_k) = \frac{-(\mathbf{a}_k^H \mathbf{Q}_k^{-1} \mathbf{a}_k)^2 + 2 \frac{\mathbf{a}_k^H \mathbf{Q}_k^{-1} \mathbf{\Gamma} \mathbf{Q}_k^{-1} \mathbf{a}_k}{(1 + P_k \mathbf{a}_k^H \mathbf{Q}_k^{-1} \mathbf{a}_k)} \mathbf{a}_k^H \mathbf{Q}_k^{-1} \mathbf{a}_k}{(1 + P_k \mathbf{a}_k^H \mathbf{Q}_k^{-1} \mathbf{a}_k)^2}$$

and hence $f''(\tilde{P}_k)$ is

$$f''(\tilde{P}_k) = \frac{(\mathbf{a}_k^H \mathbf{Q}_k^{-1} \mathbf{a}_k)^2}{(1 + \tilde{P}_k \mathbf{a}_k^H \mathbf{Q}_k^{-1} \mathbf{a}_k)^2} \quad (28)$$

which is strictly positive. This means that \tilde{P}_k is the unique minimizer of $f(P_k)$. In principle, \tilde{P}_k may be negative. However, since P_k represents power, it should be nonnegative. The minimizer of $f(P_k)$ subject to the constraint $P_k \geq 0$ is

$$\hat{P}_k = \max(0, \tilde{P}_k) \quad (29)$$

since \tilde{P}_k is the unique minimizer of $f(P_k)$ (when $\tilde{P}_k < 0$, $f(0) \leq f(P_k)$ for $\forall P_k \geq 0$).

By using the matrix inversion lemma in (27) to replace \mathbf{Q}_k by \mathbf{R} , we get

$$\hat{P}_k = \max\left(0, P_k + \frac{\mathbf{a}_k^H \mathbf{R}^{-1} (\mathbf{\Gamma} - \mathbf{R}) \mathbf{R}^{-1} \mathbf{a}_k}{(\mathbf{a}_k^H \mathbf{R}^{-1} \mathbf{a}_k)^2}\right). \quad (30)$$

Computing \hat{P}_k requires knowledge of P_k and \mathbf{R} (recall that $\mathbf{R} = \mathbf{A}(\theta)\mathbf{P}\mathbf{A}^H(\theta)$, where \mathbf{P} is a diagonal matrix with $\{P_k\}$ on its diagonal). Therefore the algorithm must be implemented iteratively; the initialization is done with DAS. IAA-ML will be locally convergent if \mathbf{R} is recalculated after each P_k is updated because of the cyclical maximization of the likelihood function.

Note that (30) can be written as (assuming $\tilde{P}_k \geq 0$)

$$\hat{P}_k = \frac{\mathbf{a}_k^H \mathbf{R}^{-1} \mathbf{\Gamma} \mathbf{R}^{-1} \mathbf{a}_k}{(\mathbf{a}_k^H \mathbf{R}^{-1} \mathbf{a}_k)^2} + P_k - \frac{1}{(\mathbf{a}_k^H \mathbf{R}^{-1} \mathbf{a}_k)}. \quad (31)$$

By the properties of SCB, $P_k \approx 1/(\mathbf{a}_k^H \mathbf{R}^{-1} \mathbf{a}_k)$ [6, 43]. Hence an approximate solution of (31) is

$$\hat{P}_k = \frac{\mathbf{a}_k^H \mathbf{R}^{-1} \mathbf{\Gamma} \mathbf{R}^{-1} \mathbf{a}_k}{(\mathbf{a}_k^H \mathbf{R}^{-1} \mathbf{a}_k)^2}, \quad k = 1, \dots, K. \quad (32)$$

Iterating this equation by building \mathbf{R} from the latest estimate of $\{P_k\}$, we get IAA-APES. This approximation has two advantages. First the \hat{P}_k in (32) is guaranteed to be nonnegative, and it alleviates the need for the procedure in (29). Secondly when $\{P_k\}$ is accurate, the difference $P_k - 1/(\mathbf{a}_k^H \mathbf{R}^{-1} \mathbf{a}_k)$ in (31) is small, as discussed above. When $\{P_k\}$ is inaccurate, however, this difference may not be small, and forcing the difference to zero may provide a better estimate of P_k . (IAA-ML tends to work well when the snapshot number is large. It is not considered in the numerical examples because of our focus on cases with few snapshots.) Since IAA-APES can be obtained as a close approximation to IAA-ML, which is locally convergent, IAA-APES is expected to also enjoy local convergence. We have never come across an example where IAA-APES did not converge; however, the search for a convergence proof could be a useful direction for future work.

ACKNOWLEDGMENT

We thank Professor Aaron Lanterman for his useful comments on the revisions of a former version of this paper.

REFERENCES

- [1] Li, J., and Stoica P. (Eds.)
Robust Adaptive Beamforming.
New York: Wiley, 2005.
- [2] Capon, J.
High resolution frequency-wavenumber spectrum analysis.
Proceedings of the IEEE, **57** (Aug. 1969), 1408–1418.
- [3] Schmidt, R. O.
Multiple emitter location and signal parameter estimation.
IEEE Transactions on Antennas and Propagation, **AP-34**, 3 (Mar. 1986), 276–280.
- [4] Stoica, P., and Nehorai, A.
MUSIC, maximum likelihood, and Cramer-Rao bound.
IEEE Transactions on Acoustics, Speech, and Signal Processing, **5** (May 1989), 720–741.
- [5] Van Trees, H. L.
Optimum Array Processing: Part IV of Detection, Estimation, and Modulation Theory.
New York: Wiley, 2002.
- [6] Li, J., Stoica, P., and Wang, Z.
On robust Capon beamforming and diagonal loading.
IEEE Transactions on Signal Processing, **51**, 7 (July 2003), 1702–1715.
- [7] Swindlehurst, A. L., and Kailath, T.
A performance analysis of subspace-based methods in the presence of model errors, Part I: The MUSIC algorithm.
IEEE Transactions on Signal Processing, **40**, 7 (July 1992), 1758–1773.
- [8] Stoica, P., Wang, Z., and Li, J.
Extended derivations of MUSIC in the presence of steering vector errors.
IEEE Transactions on Signal Processing, **53**, 3 (Mar. 2005), 1209–1211.
- [9] Li, J., Stoica, P., and Wang, Z.
Doubly constrained robust Capon beamformer.
IEEE Transactions on Signal Processing, **52**, 9 (Sept. 2004), 2407–2423.
- [10] Baggeroer, A. B., and Cox, H.
Passive sonar limits upon nulling multiple moving ships with large aperture arrays.
In *Proceedings of the 33th Asilomar Conference on Signals, Systems and Computers*, vol. 1, 1999, 103–108.
- [11] Kraay, A. L., and Baggeroer, A. B.
A physically constrained maximum-likelihood method for snapshot-deficient adaptive array processing.
IEEE Transactions on Signal Processing, **55**, 8 (Aug. 2007), 4048–4063.
- [12] Donoho, D. L., and Elad, M.
Optimally sparse representation in general (nonorthogonal) dictionaries via l^1 minimization.
Proceedings of the National Academy of Sciences, **100**, 5 (Mar. 2000), 2197–2202.
- [13] Tropp, J. A.
Just relax: Convex programming methods for identifying sparse signals.
IEEE Transactions on Information Theory, **51**, 3 (Mar. 2006), 1030–1051.
- [14] Fuchs, J. J.
On sparse representations in arbitrary redundant bases.
IEEE Transactions on Information Theory, **50**, 6 (2004), 1341–1344.
- [15] Fuchs, J. J.
Recovery of exact sparse representations in the presence of bounded noise.
IEEE Transactions on Information Theory, **51**, 10 (2005), 3601–3608.
- [16] Tibshirani, R.
Regression shrinkage and selection via the lasso.
Journal of the Royal Statistical Society, **58**, 1 (1996), 267–288.
- [17] Chen, S. S., Donoho, D. L., and Saunders, M. A.
Atomic decomposition by basis pursuit.
SIAM Journal on Scientific Computing, **20**, 1 (1998), 33–61.
- [18] Gorodnitsky, I. F., and Rao, B. D.
Sparse signal reconstruction from limited data using FOCUSS: A re-weighted minimum norm algorithm.
IEEE Transactions on Signal Processing, **45**, 3 (1997), 600–616.
- [19] Tipping, M. E.
Sparse Bayesian learning and the relevance vector machine.
Journal of Machine Learning Research, **1** (2001), 211–244.
- [20] Wipf, D. P., and Rao, B. D.
Sparse Bayesian learning for basis selection.
IEEE Transactions on Signal Processing, **52**, 8 (2004), 2153–2164.
- [21] Figueiredo, M. A. T.
Adaptive sparseness for supervised learning.
IEEE Transactions on Pattern Analysis and Machine Intelligence, **25**, 9 (2003), 1150–1159.
- [22] Cotter, S. F., Rao, B. D., Kjersti, E., and Kreutz-Delgado, K.
Sparse solutions to linear inverse problems with multiple measurement vectors.
IEEE Transactions on Signal Processing, **53**, 7 (2005), 2477–2488.
- [23] Wipf, D. P., and Rao, B. D.
An empirical Bayesian strategy for solving the simultaneous sparse approximation problem.
IEEE Transactions on Signal Processing, **55**, 7 (2007), 3704–3716.
- [24] Malioutov, D. M.
A sparse signal reconstruction perspective for source localization with sensor arrays.
M.S. thesis, Massachusetts Institute of Technology, Cambridge, MA, July 2003.
- [25] Malioutov, D. M., Çetin, M., and Willsky, A. S.
A sparse signal reconstruction perspective for source localization with sensor arrays.
IEEE Transactions on Signal Processing, **53**, 8 (2005), 3010–3022.
- [26] Model, D., and Zibulevsky, M.
Signal reconstruction in sensor arrays using sparse representations.
Signal Processing, **86**, 3 (2006), 624–638.
- [27] Fuchs, J. J.
Linear programming in spectral estimation. Application to array processing.
In *Proceedings of the IEEE Conference on Acoustics, Speech, and Signal Processing*, 1996, 3161–3164.
- [28] Fuchs, J. J.
On the application of the global matched filter to DOA estimation with uniform circular arrays.
IEEE Transactions on Signal Processing, **49**, 4 (2001), 702–709.
- [29] Yardibi, T., Li, J., Stoica, P., and Cattafesta, L. N.
Sparsity constrained deconvolution approaches for acoustic source mapping.
Journal of the Acoustical Society of America, **123**, 5 (May 2008), 2631–2642.

- [30] Sacchi, M. D., Ulrych, T. J., and Walker, C. J.
Interpolation and extrapolation using a high-resolution discrete Fourier transform.
IEEE Transactions on Signal Processing, **46**, 1 (Jan.1998), 31–38.
- [31] Jeffs, B.
Sparse inverse solution methods for signal and image processing applications.
In *Proceedings of the IEEE International Conference on Acoustics, Speech and Signal Processing*, **3** (May 1998), 1885–1888.
- [32] Ting, M., Raich, R., and Hero, A.
Sparse image reconstruction using sparse priors.
Presented at the IEEE International Conference on Image Processing, Atlanta, GA, Oct. 2006.
- [33] Raich, R., and Hero, A.
Sparse image reconstruction for partially known blur functions.
Presented at the IEEE International Conference on Image Processing, Atlanta, GA, Oct. 2006.
- [34] Li, J., and Stoica, P.
An adaptive filtering approach to spectral estimation and SAR imaging.
IEEE Transactions on Signal Processing, **44**, 6 (June 1996), 1469–1484.
- [35] Stoica, P., Li, H., and Li, J.
A new derivation of the APES filter.
IEEE Signal Processing Letters, **6**, 8 (Aug. 1999), 205–206.
- [36] Stoica, P., Jakobsson, A., and Li, J.
Capon, APES and matched-filterbank spectral estimation.
Signal Processing, **66**, 1 (Apr. 1998), 45–59.
- [37] Schwarz, G.
Estimating the dimension of a model.
The Annals of Statistics, **6**, 2 (1978), 461–464.
- [38] Stoica, P., and Selén, Y.
Model-order selection: A review of information criterion rules.
IEEE Signal Processing Magazine, **21**, 4 (July 2004), 36–47.
- [39] Li, J., and Stoica, P.
Efficient mixed-spectrum estimation with applications to target feature extraction.
IEEE Transactions on Signal Processing, **44**, 2 (Feb. 1996), 281–295.
- [40] Li, J., Stoica, P., and Zheng, D.
Angle and waveform estimation via RELAX.
IEEE Transactions on Aerospace and Electronic Systems, **33** (July 1997), 1077–1087.
- [41] Humphreys, Jr., W. M., Brooks, T. F., Hunter, Jr., W. W., and Meadows, K. R.
Design and use of microphone directional arrays for aeroacoustic measurements.
Presented at the 36th Aerospace Sciences Meeting and Exhibit, Reno, NV, Jan. 1998; AIAA Paper 98-0471.
- [42] Baggeroer, A. B.
Sonar arrays and array processing.
In *Proceedings of AIP Conference*, vol. 1, Apr. 2005, 3–24.
- [43] Stoica, P., and Moses, R. L.
Spectral Analysis of Signals.
Upper Saddle River, NJ: Prentice-Hall, 2005.
- [44] Labit, Y., Peaucelle, D., and Henrion, D.
SEDUMI interface 1.02—A tool for solving LMI problems with SEDUMI.
In *Proceedings of the IEEE International Symposium on Computer*, Glasgow, UK, Sept. 2002, 272–277.
- [45] Brooks, T. F., and Humphreys, Jr., W. M.
A deconvolution approach for the mapping of acoustic sources (DAMAS) determined from phased microphone arrays.
Journal of Sound and Vibration, **294** (July 2006), 856–879.
- [46] Nelder, J. A., and Mead, R.
A simplex method for function minimization.
Computer Journal, **7** (1965), 308–313.
- [47] Lagarias, J. C., Reeds, J. A., Wright, M. H., and Wright, P. E.
Convergence properties of the Nelder-Mead simplex method in low dimensions.
SIAM Journal of Optimization, **9**, 1 (1998), 112–147.
- [48] Blunt, S. D., and Gerlach, K.
Adaptive pulse compression via MMSE estimation.
IEEE Transactions on Aerospace and Electronic Systems, **42**, 2 (Apr. 2006), 572–584.
- [49] Stoica, P., Li, J., and Xue, M.
Transmit codes and receive filters for pulse compression radar systems.
IEEE Signal Processing Magazine, **25**, 6 (Nov. 2008).
- [50] Stoica, P., Li, J., and Xue, M.
On sequences with good correlation properties: A new perspective.
Presented at the 2007 IEEE Information Theory Workshop on Information Theory for Wireless Networks, Bergen, Norway, July 2007.
- [51] Stutt, C., and Spafford, L.
A “best” mismatched filter response for radar clutter discrimination.
IEEE Transactions on Information Theory, **14**, 2 (Mar. 1968), 280–287.
- [52] Ackroyd, M. H., and Ghani, F.
Optimum mismatched filters for sidelobe suppression.
IEEE Transactions on Aerospace and Electronic Systems, **9**, 2 (Mar. 1973), 214–218.
- [53] Nunn, C.
Constrained optimization applied to pulse compression codes, and filters.
In *Proceedings of the IEEE International Radar Conference*, Arlington, VA, May 9–12, 2005, 190–194.
- [54] Levanon, N.
Cross-correlation of long binary signals with longer mismatched filters.
IEEE Proceedings—Radar, Sonar, and Navigation, **152**, 6 (Dec. 2005), 377–382.
- [55] Blunt, S. D., Smith, K. J., and Gerlach, K.
Doppler-compensated adaptive pulse compression.
In *Proceedings of the IEEE Conference on Radar*, Verona, NY, Apr. 24–27, 2006, 114–119.
- [56] Fuchs, J. J.
Convergence of a sparse representations algorithm applicable to real or complex data.
IEEE Journal of Selected Topics in Signal Processing, **1**, 4 (2007), 598–605.
- [57] Preisig, J. C., and Deane, G. B.
Surface wave focusing and acoustic communications in the surf zone.
Journal of the Acoustical Society of America, **116**, 4 (Oct. 2004), 2067–2080.
- [58] Preisig, J. C.
Performance analysis of adaptive equalization for coherent acoustic communications in the time-varying ocean environment.
Journal of the Acoustical Society of America, **118**, 1 (July 2005), 263–278.

- [59] Li, J., Zheng, X., and Stoica, P.
MIMO SAR imaging: Signal synthesis and receiver design.
Presented at the 2nd International Workshop on Computational Advances in Multi-Sensor Adaptive Processing, St. Thomas, US Virgin Islands, 2007.
- [60] Li, J., Stoica, P., and Zheng, X.
Signal synthesis and receiver design for MIMO radar imaging.
IEEE Transactions on Signal Processing, **56**, 8 (Aug. 2008), 3959–3968.
- [61] Kocic, M., Brady, D., and Stojanovic, M.
Sparse equalization for real-time digital underwater acoustic communications.
In *Proceedings of the IEEE/MTS Oceans Conference*, vol. 3, Oct. 1995, 1417–1422.
- [62] Stojanovic, M.
Recent advances in high-speed underwater acoustic communications.
IEEE Journal of Oceanic Engineering, **21**, 2 (Apr. 1996), 125–136.
- [63] Stojanovic, M., Freitag, L., and Johnson, M.
Channel-estimation-based adaptive equalization of underwater acoustic signals.
In *Proceedings of the IEEE/MTS Oceans Conference*, vol. 2, Sept. 1999, 985–990.
- [64] Carbonelli, C., Vedantam, S., and Mitra, U.
Sparse channel estimation with zero tap detection.
IEEE Transactions on Wireless Communications, **6**, 5 (2007), 1743–1753.
- [65] Mallat, S., and Zhang, Z.
Matching pursuits with time-frequency dictionaries.
IEEE Transactions on Signal Processing, **41**, 12 (1993), 3397–3415.
- [66] Natarajan, B. K.
Sparse approximation solutions to linear systems.
SIAM Journal of Computing, **24** (1995), 227–234.
- [67] Cotter, S. F., Adler, R., Rao, R. D., and Kreutz-Delgado, K.
Forward sequential algorithms for best basis selection.
IEEE Proceedings of Vision, Image and Signal Processing, **146**, 5 (Oct. 1999), 235–244.
- [68] Li, W.
Estimation and tracking of rapidly time-varying broadband acoustic communication channels.
Ph.D. dissertation, Massachusetts Institute of Technology, Cambridge, MA, 2005.
- [69] Li, W., and Preisig, J. C.
Estimation and equalization of rapidly varying sparse acoustic communication channels.
In *Proceedings of the IEEE/MTS Oceans Conference*, Sept. 2006, 1–6.
- [70] Li, W., and Preisig, J. C.
Estimation of rapidly time-varying sparse channels.
IEEE Journal of Oceanic Engineering, **32**, 4 (2007), 927–939.
- [71] Cotter, S. F., and Rao, B. D.
The adaptive matching pursuit algorithm for estimation and equalization of sparse time-varying channels.
In *Proceedings of the 25th Asilomar Conference on Signals, Systems and Computers*, vol. 2, Pacific Grove, CA, Oct. 2000, 1772–1776.
- [72] Cotter, S. F., and Rao, B. D.
Sparse channel estimation via matching pursuit with application to equalization.
IEEE Transactions on Communications, **50**, 3 (Mar. 2002), 374–377.
- [73] Löfberg, J.
YALMIP: A toolbox for modeling and optimization in MATLAB.
In *Proceedings of the 2004 IEEE International Symposium on Computer Aided Control Systems Design*, Sept. 2004, 284–289.
- [74] Proakis, J. G.
Digital Communications (4th ed.).
Columbus, OH: McGraw-Hill, 2001.
- [75] James, W., and Stein, C.
Estimation with quadratic loss.
In *Proceedings of the Fourth Berkeley Symposium on Mathematical Statistics Probability*, vol. 1, 1961, 361–380.
- [76] Dey, D. K., and Srinivasan, C.
Estimation of a covariance matrix under Stein’s loss.
The Annals of Statistics, **13**, 4 (Dec. 1985), 1581–1591.



Tarik Yardibi (S'08) received his B.S. degree from Hacettepe University, Ankara, Turkey in 2004 and his M.S. degree from Bilkent University, Ankara, Turkey in 2006, both in electrical engineering.

He is currently pursuing a Ph.D. degree at the Spectral Analysis Laboratory at the University of Florida, Gainesville. His research interests include statistical signal processing, sensor array processing, aeroacoustic measurements, and sparse signal representations.

Jian Li (S'87—M'91—SM'97—F'05) received her M.Sc. and Ph.D. degrees in electrical engineering from The Ohio State University, Columbus, in 1987 and 1991, respectively.

From April 1991 to June 1991, she was an adjunct assistant professor with the Department of Electrical Engineering, The Ohio State University, Columbus. From July 1991 to June 1993, she was an assistant professor with the Department of Electrical Engineering, University of Kentucky, Lexington. Since August 1993, she has been with the Department of Electrical and Computer Engineering, University of Florida, Gainesville, where she is currently a professor. In Fall 2007, she was on sabbatical leave at MIT, Cambridge, Massachusetts. Her current research interests include spectral estimation, statistical and array signal processing, and their applications.

Dr. Li is a Fellow of IET. She is a member of Sigma Xi and Phi Kappa Phi. She received the 1994 National Science Foundation Young Investigator Award and the 1996 Office of Naval Research Young Investigator Award. She was an executive committee member of the 2002 International Conference on Acoustics, Speech, and Signal Processing, Orlando, FL, May 2002. She was an Associate Editor of the *IEEE Transactions on Signal Processing* from 1999 to 2005, an Associate Editor of the *IEEE Signal Processing Magazine* from 2003 to 2005, and a member of the Editorial Board of *Signal Processing*, a publication of the European Association for Signal Processing (EURASIP), from 2005 to 2007. She has been a member of the Editorial Board of *Digital Signal Processing—A Review Journal*, a publication of Elsevier, since 2006. She is presently a member of the Sensor Array and Multichannel (SAM) Technical Committee of IEEE Signal Processing Society. She is a coauthor of papers that have received the First and Second Place Best Student Paper Awards, respectively, at the 2005 and 2007 Annual Asilomar Conferences on Signals, Systems, and Computers in Pacific Grove, CA. She is also a coauthor of the paper that has received the M. Barry Carlton Award for the best paper published in *IEEE Transactions on Aerospace and Electronic Systems* in 2005.



Petre Stoica (SM'91—F'94) received the D.Sc. degree in automatic control from the Polytechnic Institute of Bucharest (BPI), Bucharest, Romania, in 1979 and an honorary doctorate degree in science from Uppsala University (UU), Uppsala, Sweden, in 1993.

He is a Professor of Systems Modeling with the Division of Systems and Control, the Department of Information Technology at UU. Previously, he was a Professor of System Identification and Signal Processing with the Faculty of Automatic Control and Computers at BPI. He held longer visiting positions with Eindhoven University of Technology, Eindhoven, The Netherlands; Chalmers University of Technology, Gothenburg, Sweden (where he held a Jubilee Visiting Professorship); UU; University of Florida, Gainesville, FL; and Stanford University, Stanford, CA. His main scientific interests are in the areas of system identification, time series analysis and prediction, statistical signal and array processing, spectral analysis, wireless communications, and radar signal processing.

Dr. Stoica has published nine books, ten book chapters, and some 500 papers in archival journals and conference records. The most recent book he coauthored, with R. Moses, is *Spectral Analysis of Signals* (Prentice-Hall, 2005). He is on the editorial boards of six journals: *Journal of Forecasting*, *Signal Processing*, *Circuits, Signals, and Signal Processing*, *Digital Signal Processing*, *CA Review Journal*, *Signal Processing Magazine*, and *Multidimensional Systems and Signal Processing*. He was a coquest editor for several special issues on system identification, signal processing, spectral analysis, and radar for some of the aforementioned journals, as well as for *IEEE Proceedings*. He was corecipient of the IEEE ASSP Senior Award for a paper on statistical aspects of array signal processing. He was also recipient of the Technical Achievement Award of the IEEE Signal Processing Society. In 1998, he was the recipient of a Senior Individual Grant Award of the Swedish Foundation for Strategic Research. He was also corecipient of the 1998 EURASIP Best Paper Award for Signal Processing for a work on parameter estimation of exponential signals with time-varying amplitude, a 1999 IEEE Signal Processing Society Best Paper Award for a paper on parameter and rank estimation of reduced-rank regression, a 2000 IEEE Third Millennium Medal, and the 2000 W. R. G. Baker Prize Paper Award for a paper on maximum likelihood methods for radar. He has been a member of the international program committees of many topical conferences. From 1981 to 1986, he was a Director of the International Time-Series Analysis and Forecasting Society, and he was also a member of the IFAC Technical Committee on Modeling, Identification, and Signal Processing. He is also a member of the Royal Swedish Academy of Engineering Sciences, an honorary member of the Romanian Academy, and a fellow of the Royal Statistical Society.

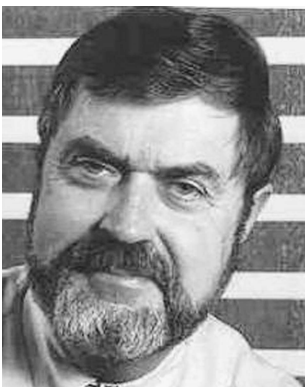


Ming Xue (S'08) received his B.S. degree in electrical engineering from the University of Science and Technology of China, Hefei, China in 2006.

He is working towards a Ph.D. degree in the Department of Electrical and Computer Engineering, University of Florida, Gainesville. His research interests include statistical signal processing and its applications.

Arthur B. Baggeroer (S'62—M'68—SM'87—F'89) received the degrees of B.S.E.E. from Purdue University in 1963 and Sc.D. from MIT in 1968. He is a Ford Professor of Engineering in the Departments of Mechanical Engineering and Electrical Engineering & Computer Science at the Massachusetts Institute of Technology. He was been a consultant to the Chief of Naval Research at the NATO SACLANT Center (now NURC) in 1977 and a Cecil and Ida Green Scholar at the Scripps Institution of Oceanography in 1990 while on sabbatical leaves.

Dr. Baggeroer is a Fellow of the Acoustical Society of America. He received the IEEE Oceanic Engineering Society Distinguished Technical Achievement Award in 1991, was an elected member of the Executive Council of the Acoustical Society from 1994–1997, and was awarded the Rayleigh-Helmholtz Medal from the Acoustical Society in 2003. He was elected to the National Academy of Engineering in 1995 and awarded a Secretary of the Navy/Chief of Naval Operations Chair in Oceanographic Science in 1998. He serves as a senior advisor to the Navy on numerous committees and panels. He recently chaired the NSB panel on Distributed Remote Surveillance (DRS). Professor Baggeroer was awarded the “Distinguished Alumni Award” of the Department of Electrical and Computer Engineering from his alma mater, Purdue University. He was recently awarded the ADM Charles Martel–David Bushnell Award by NDIA for “outstanding technical contributions to the defense of the US in the field of Undersea Warfare.” He has been chief scientist on fifteen oceanographic cruises with seven in the Arctic Ocean. His research has concerned signal and array processing for sonar, radar and seismic systems, ocean acoustic telemetry, global acoustics for ocean thermometry and matched field array processing. He also has had long affiliations with the Woods Hole Oceanographic Institution where he was Director of the MIT–Woods Hole Joint Program from 1983–1988 and the MIT–Lincoln Laboratory. Finally, he was elected four times to be a member of the School Committee for the Town of Westwood, MA (1978–1990) and was elected to be chairman four times.



Some of the Navy Committees he has been involved in are: 1) the Naval Studies Board, 2) the Ocean Studies Board (both for six years), 3) the Submarine Superiority Technical Advisory Group (he was a member of the original committee for ADM Demars which led to APB/ARCI), 4) the Fixed Surveillance Systems Technical Advisory Group, 5) the SSIPT for N84 (twice), 6) the “Red Team” special programs component for the Way Ahead for ASW, 7) an advisory panel member for several programs for the Navy and DARPA, and 8) the Naval Research Advisory Committee.